別紙4-(2)

参考資料

書籍

著者氏名	論文タイトル名	書籍全体の編集者名	書　籍　名	出版社名	出版地	出版年	ページ
Ageta H, Tsuchida K	Multifunctional Roles of Activins in the Brain	Litwack G.	Activins and Inhibins, Vitaminsand Hormones Vol 85	Elsevier Inc.	London, UK	2011	185-206

雑誌

発表者氏名	論文タイトル名	発表誌名	巻号	ページ	出版年
Ageta H, Ikegami S, Miura M, Masuda M, Migishima R, Hino T, Takashima N, Murayama A, Sugino H, Setou M, Kida S, Yokoyama M, Hasegawa Y, Tsuchida K, Aosaki T, Inokuchi K.	Activin plays a key role in the maintenance of long-term memory and late-LTP.	Learning and Memory	17(4)	176-185	2010
Lee SJ, Lee YS, Zimmers TA, Soleimani A, Matzuk MM, Tsuchida K, Cohn RD, BartonER.	Regulation of Muscle Mass by Follistatin and Activins	Mol.Endocrinol.	24(10)	1998-2008	2010
上住聡芳、中谷直史、常陸圭介、土田邦博	老化や疾患における骨格筋の萎縮と治療への応用	基礎老化研究	34(4)	5-11	2010

Ⅳ. 研究成果の刊行物・別刷
（参考資料）

INTERNAL MEDICINE

□ ORIGINAL ARTICLE □

Rapid Screening for Japanese Dysferlinopathy by Fluorescent Primer Extension

Saori Hayashi[1], Yutaka Ohsawa[1], Toshiaki Takahashi[2], Naoki Suzuki[3], Tadashi Okada[1], Mitsue Rikimaru[1], Tatsufumi Murakami[1], Masashi Aoki[3] and Yoshihide Sunada[1]

Abstract

Objective Mutations in the dysferlin gene cause limb-girdle muscular dystrophy (LGMD) 2B and Miyoshi myopathy (MM), which are collectively named dysferlinopathy. Dysferlinopathy is the most frequent type of LGMD in the Japanese population. Molecular genetic analysis is essential for the diagnosis of dysferlinopathy because of its variable immunohistochemical patterns of biopsied muscles, including patterns similar to normal controls. The analysis of the entire dysferlin gene however, is time-consuming and laborious; therefore a simple and rapid screening method to detect hot spot mutations in the dysferlin gene is essential for the diagnosis of dysferlinopathy.

Methods We previously showed that 4 mutations, c.937+1G>A, c.1566C>G, c.2997G>T and c.3373delG account for 50% of all the mutations identified in Japanese dysferlinopathy patients. We performed a one-tube multiplex PCR, followed by extension of primers for each mutation with a fluorescence-labeled dideoxynucleotide to screen the 4 hot spot mutations.

Results The multiplex primer-extension reaction was developed on samples of known mutations. The extension products were represented as 4 different peaks that corresponded to a mutated nucleotide on electropherogram. Using the developed screening method, we were able to detect mutations in these hot spots in 3 samples out of 8 clinically suspected LGMD2B/MM patients in only approximately 8 hours. These 3 cases were definitely diagnosed as LGMD2B/MM by exonic sequencing.

Conclusion We have developed a simple and rapid screening method which could facilitate the definitive diagnosis of dysferlinopathy, contributing to an understanding of the genotype-phenotype correlations for dysferlinopathy.

Key words: limb-girdle muscular dystrophy (LGMD) 2B, Miyoshi myopathy (MM), dysferlinopathy, mutational hot spots, fluorescent primer extension

(Intern Med 49: 2693-2696, 2010)
(DOI: 10.2169/internalmedicine.49.3771)

Introduction

The loss of dysferlin, resulting from homozygous or compound heterozygous mutations in the dysferlin gene (GeneID: 8291) causes dysferlinopathy, including autosomal recessive limb-girdle muscular dystrophy (LGMD) 2B, Miyoshi myopathy (MM) and distal anterior compartment myopathy (1, 2). Dysferlinopathy is the most frequent type of LGMD in the Japanese population (personal communication by Dr. Yukiko Hayashi, National Center of Neurology and Psychiatry). Commonly, the diagnosis of dysferlinopathy is made by immunohistochemistry (IHC). However, IHC analyses with anti-dysferlin antibodies in LGMD2B/MM patients show multiple staining patterns, including patterns similar to normal controls. In addition, other types of LGMD, such as LGMD2A and LGMD1C sometimes show altered immunostaining patterns similar to LGMD2B/MM (3). Therefore, molecular genetic analysis is essential for the diagnosis of dysferlinopathy. Because the dysferlin

[1]Department of Neurology, Kawasaki Medical School, Kurashiki, [2]Department of Neurology, Nishitaga National Hospital, Sendai and [3]Department of Neurology, Tohoku University School of Medicine, Sendai
Received for publication April 7, 2010; Accepted for publication August 26, 2010
Correspondence to Dr. Yoshihide Sunada, ysunada@med.kawasaki-m.ac.jp

Table 1. Clinical Features of 10 Patients

Patient No.	Sex	Age at onset, y	Clinical diagnosis	Hot spot mutations by primer extension	Other mutations by exonic sequencing
1	F	21	LGMD2B	c.2997G>T + c.2997G>T	—
2	M	56	LGMD2B*	—	ND
3	M	18	LGMD2B*	—	ND
4	M	15	MM	c.1566C>G	c.265C>T
5	F	56	MM*	—	ND
6	F	66	MM**	—	ND
7	M	18	MM	—	c.3112C>T + c.5226C>T
8	M	15	MM	c.3373delG	c.1321C>T
9	M	60	other LGMD	—	ND
10	F	21	other LGMD	—	ND

ND: not determined. Dysferlin immunoreactivity: *absent, **faint.

Table 2. Primers Used for PCR and Extension Reaction

Mutations (No. of Exon)	Primer sequences	Size Bp
c.937+1G>A	F-ccacactttatttaacgctttggcgg	
(Exon 10)	R-cagaaccaaaatgcaaggatacgg	
	E-accatttacagagagcccc	19
c.1566C>G	F-cgacccctctgattgccacttgtg	
(Exon 18)	R-ggcatcctgcccttgccaggg	
	E-aaaaaccacttttgggccctgcta	24
c.2997G>T	F-tcctctcattgcttgcctgttcgg	
(Exon 28)	R-ttgagagcttgccggggatgg	
	E-aaaaaaaaaagtgggaagatgaggaatg	28
c.3373delG	F-atctaactctctgggctagtc	
(Exon 31)	R-tatcaccccatagaggcctcgaag	
	E-aaaaaaaaaaaagcgtgatggatgacaagagt	32

F: Forward primer for exonic PCR, R: Reverse primer for exonic PCR, E: Extension primer

gene consists of 55 exons spanning more than 150 kb, molecular genetic analysis of the entire gene is time-consuming and laborious. Therefore, an easier method to screen for common mutations is now required to facilitate DNA-based diagnosis of dysferlinopathy. We previously showed that 4 mutations, c.937+1G>A, c.1566C>G, c.2997G>T and c.3373delG account for 50% of all the mutations identified in Japanese dysferlinopathy patients (4). In this study, we have developed a simple and rapid screening method to detect these mutational hot spots in the dysferlin gene using fluorescent primer extension.

Materials and Methods

DNA samples

To develop a new screening method, we collected control DNA samples from patients genetically diagnosed with dysferlinopathy. Genomic DNAs from patients with MM (n=8), carrying the homozygous and heterozygous mutations at the hot spots c.937+1G>A, c.1566C>G, c.2997G>T, and c.3373delG in the dysferlin gene were used as positive controls, and 4 negative controls were applied to this study. Description of sequence variations are modified basically as recommended by the Ad-Hoc Committee for Mutation Nomenclature (AHCMN), with the recently suggested additions as follows; G1310A to c.937+1G>A (p.?), C1939G to c.1566C>G (p.Y522X), G3370T to c.2997G>T (p.W999C), and 3746delG to c.3373delG (p.E1125KfsX1134) (5).

To test the usefulness of the newly developed method, we further collected 8 DNA samples from patients who were clinically suspected to have LGMD2B/MM based on the typical clinical picture and the muscle biopsy finding of dysferlin deficiency and 2 other LGMD patients as shown in Table 1.

PCR

Pairs of primers were designed to amplify DNA fragments containing the 4 mutational hot spots (Table 2). Multiplex PCR amplification was performed in 1 tube, with 35 cycles of 94°C for 15 second, 55°C for 30 second and 72°C for 1 minute. The resulting PCR products were purified using a PCR purification kit (Qiagen, Hilden, Germany).

Fluorescent primer-extension

Using purified PCR products as the template, multiplex primer-extension reactions were performed in 1 tube to detect hot spot mutations using a SNaPshot™ Multiplex Kit (Applied Biosystems, Foster City, CA). We designed non-labeled extension primers to anneal just 5′ of the mutated nucleotide. The primer length was altered by adding poly (dA) tails at the 5′ end to vary the size of the extension products (Table 2). Once the primer anneals, a single-base extension occurs by the addition of a complementary dideoxyribonucleoside triphosphate (ddNTP) to the 3′ end of the annealed primer. In the present study, the 4 ddNTPs were fluorescently labeled as follows: black for G, green for A, blue for C and red for T. The primer extension reaction was performed in a final volume of 10 μL, containing 3 μL of

ttcattttcttttcatgtagtatcaaatgttgactgcctgtgtttccaaatgttcttcaaaaacatggtttttaatggaat

catataatgcaccacactttatttaacgctttggcggcaagagtttgatttgtgtctcctctcattgattgcagatg

gacgtgggc**accatttacagagagcccc**[G/A]tgagttctcaccactttggccgtatccttgcattttggtt

ctggaggctgattggggacactcatttggggtcctcactgtccctcctgggggttttagaatctagaggaagg

Figure 1. Sequence of exon 10 from the dysferlin gene containing the c.937+1G>A mutation. Location of the forward primer and reverse primer (underlined) in relation to the extension primer (bold).

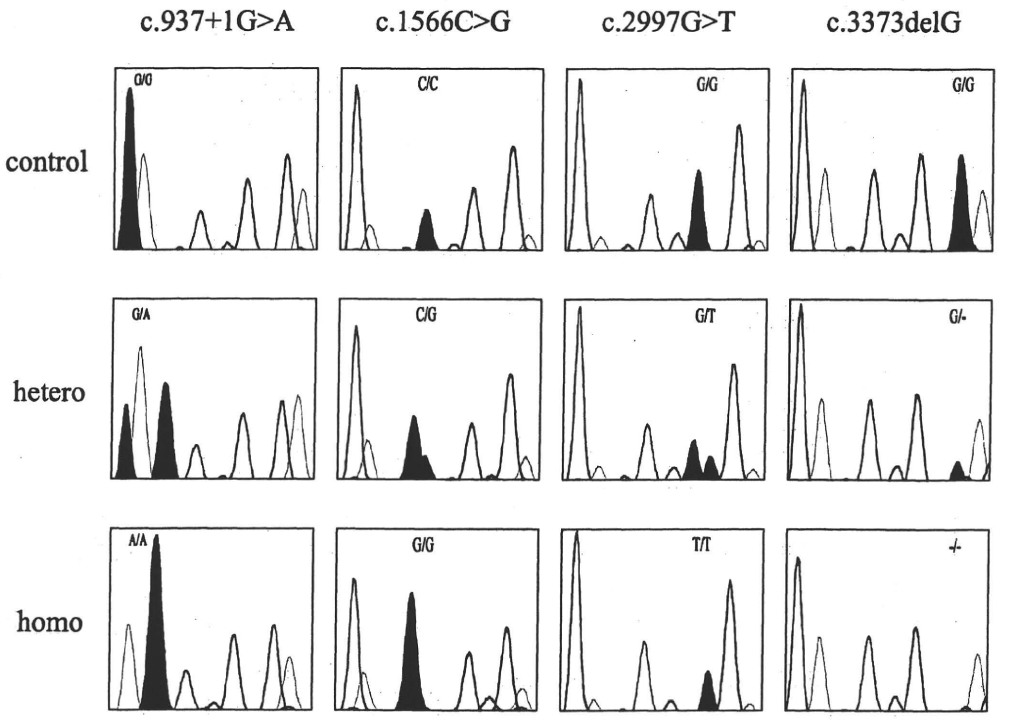

Figure 2. GeneScan electropherograms of the fluorescent primer extension reactions showing the 4 common mutations, c.937+1G>A, c.1566C>G, c.2997G>T and c.3373delG. Each genotype was determined by both the position of the peak as well as by the color of the emitted fluorescence. Hetero, heterozygous mutation; homo, homozygous mutation.

PCR product (5 ng), 5 μL of SNaPshot ready reaction mix (ddNTP terminators, DNA polymerase) and 0.2 μM of each of the extension primers corresponding to the 4 hot spots. The cycling conditions were 25 cycles of 96°C for 10 second, 50°C for 5 second and 60°C for 30 second. Post-extension treatment was conducted with 1 unit of calf intestinal alkaline phosphatase (Roche Molecular Biochemicals, Penzberg, Germany) for 60 minute at 37°C, followed by 15 minute at 75°C for enzyme inactivation. The samples were subjected to capillary electrophoresis on an ABI 310 Genetic Analyzer (Applied Biosystems) and analyzed using GeneScan software (version 3.1, Applied Biosystems).

Results

Pairs of primers for exonic PCR were designed to flank the mutated nucleotide, and the extension primers were designed to end 1 nucleotide 5′ of the mutated nuceotide as shown in Fig. 1. Electropherograms of the PCR samples after single nucleotide primer extension at the 4 hot spot mutations are shown in Fig. 2. The extension products are represented as 4 different peaks that were determined by the primer length and the incorporated fluorescently labeled ddNTP. For the c.937+1G>A mutation, the control sample produced a black peak (G), the homozygous mutant sample produced a green peak (A), and the heterozygous sample produced a black and a green peak (G and A). As expected, cases of c.1566C>G and c.2997G>T mutation were also fluorescence detected and interpreted on the electropherograms. In the case of the c.3373delG mutation, the control sample produced a black peak (G), whereas the homozygous sample showed no peak, and the heterozygous sample pro-

duced a smaller peak compared with the control sample. Direct sequencing was performed on these samples to verify the results of the fluorescent primer extension, and there was a complete concordance. The time required for the procedure was approximately 8 hour. Using the developed method, we actually screened the gene for mutations in 8 Japanese patients clinically suspected to have LGMD2B/MM and 2 other LGMD patients (Table 1). We identified 1 homozygous mutation, c.2997G>T (No.1) and 2 heterozygous mutations, c.1566C>G (No.4) and c.3373delG (No.8, total 4 alleles), out of 8 DNA samples from LGMD2B/MM patients (No.1-8, total 16 alleles). We further analyzed screening-negative alleles by exonic PCR and subsequent direct sequencing analyses. We detected mutations other than the 4 hot spots in the 2 heterozygous cases (No.4, 8) and confirmed the diagnosis of dysferlinopathy. One screening negative case (No.7) was diagnosed as dysferlinopathy by exonic sequencing alone. No mutations were detected in 2 DNA samples from other LGMD (No.9, 10) by the developed method.

Discussion

In this study, we developed a simple and rapid mutational screening method, in which both the genomic PCR and the primer extension reaction are multiplexed, and which takes only approximately 8 hour to detect mutations at any of the 4 Japanese LGMD2B/MM mutational hot spots in the dysferlin gene. This method is readily available for many laboratories, is easy to use and is suitable for a great many clinical samples. The design is flexible and more mutation sites could be added to the multiplex reactions.

Over the past 9 years, we have performed SSCP analysis of each exon of the dysferlin gene in over 150 samples from Japanese patients with clinically diagnosed or suspected LGMD2B/MM. Among them, we detected 28 different mutations in the coding region of the dysferlin gene, which were widely distributed along the entire length of the gene (unpublished data). However, using our newly developed screening method, we easily detected mutations at hot spots in 4 alleles out of 16 alleles in clinically suspected LGMD2 B/MM patients. By analyzing more samples, the sensitivity and specificity of our new method will be determined.

We propose that our rapid screening method could be applied initially to the genomic screening for dysferlinopathy, which could detect up to 50% of the mutations in Japanese dysferlinopathy patients. Further, precise analyses by SSCP, gene chip or other mutation detection methods will be necessary only in the screening-negative cases. This novel screening method could facilitate the definitive diagnosis of dysferlinopathy, thereby contributing to an understanding of the genotype-phenotype correlations for this disease.

Acknowledgement

We thank Dr. Katsuhito Adachi for providing us with information and DNA samples. This work was supported by a research grant for Nervous and Mental Disorders from the Ministry of Health, Labor and Welfare (20B-13), and by research project grants from Kawasaki Medical School (20-602 and 20-604).

References

1. Liu J, Aoki M, Illa I, et al. Dysferlin, a novel skeletal muscle gene, is mutated in Miyoshi myopathy and limb girdle muscular dystrophy. Nat Genet **20**: 31-36, 1998.
2. Illa I, Serrano-Munuera C, Gallardo E, et al. Distal anterior compartment myopathy: a dysferlin mutation causing a new muscular dystrophy phenotype. Ann Neurol **49**: 130-134, 2001.
3. Tagawa K, Ogawa M, Kawabe K, et al. Protein and gene analyses of dysferlinopathy in a large group of Japanese muscular dystrophy patients. J Neurol Sci **211**: 23-28, 2003.
4. Takahashi T, Aoki M, Tateyama M, et al. Dysferlin mutations in Japanese Miyoshi myopathy: relationship to phenotype. Neurology **60**: 1799-1804, 2003.
5. den Dunnen JT, Antonarakis SE. Mutation nomenclature extensions and suggestions to describe complex mutations: a discussion. Hum Mutat **15**: 7-12, 2000.

筋ジストロフィーの分子病態*

砂田　芳秀**

Key Words : muscular dystrophy, dystrophin, TRPV2, dysferlin, RNA splicing

はじめに

筋ジストロフィーは何らかの遺伝子異常により筋細胞が壊死・再生を繰り返しながら正常筋組織が崩壊し，臨床的には進行性の筋萎縮と筋力低下を呈する疾患の総称である．根本的な治療法の確立には，原因遺伝子の同定だけではなく，発症の分子病態の解明が必要不可欠であることはいうまでもない．1987年のジストロフィン遺伝子のクローニングを端緒として現在までに30を越える原因遺伝子が同定されており，発症にいたる分子病態の多様性が推測されるものの，その本態は未だに十分解明されてはいない．もとより，多様な分子病態をすべて網羅することは不可能であり，本講演では特に筋鞘膜の脆弱性とCa^{2+}イオンの透過性亢進，膜修復機構の異常，筋内血管拡張障害説に焦点をあてて最近の研究成果を紹介する．

I．原因蛋白の局在からみた筋ジストロフィー

分子病態を原因蛋白の細胞レベルでの局在という観点から見ると，以下の5つのグループに分類できる．(1) 細胞外マトリックス成分の異常：ラミニンα2（メロシン）欠損による先天性筋ジストロフィーMDC1A，コラーゲンVI異常によるUllrich型やBethlem myopathyなど先天性筋ジストロフィー（congenital muscular dystrophy：CMD），(2) 細胞膜関連蛋白の異常：ジストロフィン異常によるDuchenne型筋ジストロフィー（Duchenne muscular dystrophy：DMD），サルコグリカン異常による肢帯型筋ジストロフィー（LGMD）2C-F，α-ジストログリカンの糖鎖異常による福山型などのCMDやLGMD2I，細胞膜修復に関与するジスフェルリン欠損によるLGMD2B，シグナル伝達制御の関わるカベオリン3異常によるLGMD1Cなど，(3) 細胞骨格や筋原線維関連蛋白の異常：ミオティリン，タイティン，FHL-1などの異常によるLGMD，(4) 核膜関連蛋白の異常：エメリン異常によるX連鎖Emery-Dreifuss型筋ジストロフィー（EDMD），ラミンA/C異常による常染色体性EDMD，(5) その他：カルパイン3異常によるLGMD2A，ユビキチンリガーゼと推定されるTRIM32異常によるLGMD2Hなど．

こうした分子病態の中である程度コンセンサスがえられているのは①筋形質膜の脆弱性や膜修復機構の破綻による，細胞内へのCa^{2+}流入とプロテアーゼの活性化，②細胞外マトリックス成分の欠損やα-ジストログリカンのラミニン結合能の喪失など細胞内外の生存シグナルの減損であるが，最近NOS活性低下による筋肉内血管の拡張

* Molecular Pathogenesis of Muscular Dystrophies.

** 川崎医科大学神経内科学教室　Yoshihide SUNADA : Department of Neurology, Kawasaki Medical School

障害説も提唱されている．

II. 細胞膜の脆弱性とCa^{2+}イオン透過性亢進の分子機構

従来からDMDの病態として細胞膜仮説，すなわち細胞膜の脆弱性と細胞内へのCa^{2+}イオンの流入とプロテアーゼの活性化により筋細胞壊死が生じると考えられていた．ミシガン大学Metzger教授のグループはジストロフィン欠損心筋細胞を単離しマイクロカーボンを用いて筋節長だけ伸展させ，発生する張力と細胞内Ca^{2+}濃度を測定した[1]．ジストロフィン欠損心筋細胞では伸長により細胞内へCa^{2+}が流入して，過収縮が起こり心筋細胞の死滅が観察された．このようにジストロフィン欠損筋で伸長によりCa^{2+}イオンが細胞内へ流入するチャネルについては長い間わかっていなかった．最近Iwataら[2]は，ストレッチ感受性イオンチャネルであるTRPV2がCa^{2+}イオン流入のpathwayであることを見いだした．正常な骨格筋ではTRPV2は細胞質内の膜系に局在しているが，ジストロフィン欠損筋では筋鞘膜に濃縮して局在するようになる．そこで彼らは筋鞘膜に局在したTRPV2が活性化して細胞内Ca^{2+}濃度が上昇する結果，筋細胞が壊死に陥るとの作業仮説を考えた．この仮説を検証するため，ドミナントネガティブ変異を導入してTRPV2を不活化したトランスジェニックマウスを作出し，*mdx*マウスと交配して筋肉の変化を解析した．TRPV2を特異的に阻害した*mdx*マウスでは，筋細胞の壊死や線維化が有意に抑制され，筋ジストロフィー変化が改善することが示された．したがって，TRPV2の特異的な阻害薬が開発されればジストロフィノパチーの有効な治療薬として期待される．

III. 膜修復機構の異常による細胞膜の脆弱性

骨格筋は収縮と弛緩を繰り返すことから，筋鞘膜は力学的なストレスに曝されており，細胞膜が損傷を受けやすい．そこで，生体には損傷した細胞膜を修復する生理的なメカニズムが存在することが推定される．アイオワ大学のCampbellらは，三好型遠位型筋ジストロフィーやLGMD2Bの原因蛋白であるジスフェルリンが膜修復に関与することを明らかにした[3]．単一筋線維にレーザー照射により筋鞘膜損傷を与えると損傷部位にジスフェルリンが集積して，速やかに膜を修復する．一方で，ジスフェルリン欠損マウスでは膜が修復されないため，細胞外液が容易に細胞内に流入することが示された．ジスフェルリン欠損筋では損傷した筋鞘膜の直下に膜小胞が集積した像が観察されるが，修復機転において表面膜に融合できなかった小胞が集積したものと解釈できる．ジスフェルリンによる膜修復過程はCa^{2+}依存性であることが解明されている．

最近，京都大学の竹島教授のグループはジスフェルリンとは異なり，Ca^{2+}非依存性に膜修復に関与するミツグミン（MG53）という新たな分子を発見した[4]．ミツグミンのノックアウトマウスでは，筋ジストロフィー変化が観察されることから，筋ジストロフィーの発症機序への関与も推測される．また，筋ジストロフィーの新たな原因蛋白候補というだけではなく，治療薬開発の新たなシーズとしても注目されている．

IV. nNOS活性低下による血管拡張障害

熊本大学のMiikeら[5]は，電顕での観察からDMDでは早い段階から筋内血管内皮細胞が腫大して毛細血管内腔が狭小化することを指摘していた．Bredtらはジストロフィン欠損筋ではnNOSの局在が筋鞘膜から細胞質へと変化するとともに活性が低下することを見いだした[6]．しかし，nNOSノックアウトマウスでは筋障害がみられないことから，筋ジストロフィーの発症機序にnNOS活性低下がどのように関与するかは長らく不明であった．Yasuharaらは高頻度電気刺激により筋収縮運動を反復させた時，正常でみられる筋血流量の増大が*mdx*マウス（ジストロフィン欠損筋）では欠如することを見いだした[7]．さらに*mdx*マウスでは筋収縮後のNO産生が減弱していることが明らかにされた．すなわち，ジストロフィン欠損筋ではnNOS活性の減弱により筋収縮に伴う血管拡張反応を担うNO産生が低下していると推測される．そこで，NOの下流で働くcGMPを上昇させるphosphodiesterase 5（PDE5）阻害薬を*mdx*マウスに投与したところ，筋ジストロフィー変化の有意な改善が観察された．CampbellのグループもPDE5阻害薬投与により，*mdx*マウスに

おいて運動負荷後の筋血流量が顕著に増大することを示している[8].

正常な骨格筋でnNOS活性が低下しても，それだけでは筋ジストロフィーは発症しないが，ジストロフィン欠損というfirst hitの上にnNOS活性低下による筋血管拡張障害というsecond hitが加わることにより筋ジストロフィーが増悪するという，いわゆる“筋ジストロフィー発症のtwo-hit mechanism”が提唱されている.

V. RNA病としての筋ジストロフィー

スプライシングやエディティングなどのRNAプロセッシングの異常に起因する疾患はRNA病と呼ばれる．筋強直性ジストロフィーはいろいろな遺伝子のスプライシング異常によって多彩な症状を呈するRNA病であることが解明されてきた．この疾患（1型）では第19染色体のDMキナーゼ（DMPK）遺伝子の3′非翻訳領域にあるCTGリピートの異常伸長がみられるが[9]，DMPK蛋白自体には異常がない．つまり原因蛋白レベルの異常で病気が発症するわけではない．異常伸長したCTGリピートはDMPK遺伝子のRNAへの転写段階でCUGリピートとなるが，異常伸長したCUGにはMBNL1-3やCELF1-6などのRNA結合蛋白が結合する．これらのRNA結合蛋白は様々な遺伝子のmRNAへの転写過程で，スプライシングを制御している．したがって，異常伸長したCUGリピートにスプライシングを調節するRNA結合蛋白質が結合してトラップされると，正常なスプライシングの制御に支障をきたすと考えられる．この病気の特徴であるミオトニアは塩素チャネルの機能異常で生じるが，患者の筋肉では塩素チャネルCLCN1遺伝子の異常スプライシングにより幼若型CLCN1が発現している[10]．また，インスリン受容体においても，スプライシング異常により幼若型受容体が優位になっていて，おそらくインスリン耐性の原因と考えられている[11].

VI. RNAレベルの分子病態から新たな治療戦略へ

従来のような蛋白レベルの分子病態の理解だけではなくRNAレベルにおける分子病態の理解が，新たな治療法開発へのアプローチに重要になると思われる．DMDの場合DNAレベルでout-of flame欠失を修正することは困難であるが，欠失に隣接するexonをRNAへの転写段階でスプライシングによりスキップさせることでin-flame欠失に変換して軽症化を試みる，いわゆるexon skippingという治療法が注目されている．今後はDMD以外の筋ジストロフィーに対しても，このようなRNAレベルを標的とした治療戦略の応用が考えられる．したがって，重症度など臨床表現型との相関を含め，RNAレベルでの分子病態の詳細な解析が重要になると思われる.

文　献

1）Yasuda S, Townsend D, Michele DE et al : Dystrophic heart failure blocked by membrane sealant poloxamer. Nature 436 : 1025-1029, 2005

2）Iwata Y, Katanosaka Y, Arai Y et al : Dominant-negative inhibition of Ca^{2+} influx via TRPV2 ameliorates muscular dystrophy in animal models. Hum Mol Genet 18 : 824-834, 2009

3）Bansal D, Miyake K, Vogel SS et al : Defective membrane repair in dysferlin-deficient muscular dystrophy. Nature 423 : 168-172, 2003

4）Cai C, Masumiya H, Weisleder N et al : MG53 nucleates assembly of cell membrane repair machinery. Nat Cell Biol 11 : 56-64, 2009

5）Miike T, Sugino S, Ohtani Y et al : Vascular endothelial cell injury and platelet embolism in Duchenne muscular dystrophy at the preclinical stage. J Neurol Sci 82 : 67-80, 1987

6）Brenman JE, Chao DS, Xia H et al : Nitric oxide synthase complexed with dystrophin and absent from skeletal muscle sarcolemma in Duchenne muscular dystrophy. Cell 82 : 743-752, 1995

7）Asai A, Sahani N, Kaneki M et al : Primary role of functional ischemia, quantitative evidence for the two-hit mechanism, and phosphodiesterase-5 inhibitor therapy in mouse muscular dystrophy. Plos One 8 : 1-16, 2007

8）Kobayashi YM, Rader EP, Crawford RW et al : Sarcolemma-localized nNOS is required to maintain activity after mild exercise. Nature 456 : 511-515, 2008

9）Brook JD, Mila E, McCurrach HG et al : Molecular basis of myotonic dystrophy : expansion of a trinucleotide (CTG) repeat at the 3' end of a transcript encoding a protein kinase family member. Cell 68 : 799-808, 1992

10) Nezu Y, Kino Y, Sasagawa N et al : Expression of MBNL and CELF mRNA transcripts in muscles with myotonic dystrophy. Neuromuscul Disord 17 : 306-312, 2007

11) Savkur RS, Philips AV, Cooper TA : Aberrant regulation of insulin receptor alternative splicing is associated with insulin resistance in myotonic dystrophy. Nat Genet 29 : 40-47, 2001

Molecular Pathogenesis of Muscular Dystrophies

Yoshihide SUNADA

Department of Neurology, Kawasaki Medical School

Muscular dystrophy is one of the most devastating diseases for which there is no effective therapy at present. In an attempt to develop effective therapeutics, a considerable number of causative genes for the numerous types of muscular dystrophy have been identified in the last twenty years. However, uncovering causative genes alone is not enough. It is crucial to comprehend molecular pathogenesis of muscular dystrophy, focusing on the causative proteins. It is further necessary to investigate the RNA processing defects.

Muscular dystrophies can be divided into five groups depending on the subcellular localization of the causative proteins as follows : (1) the extracellular matrix proteins such as laminin $\alpha 2$ or collagen VI, (2) the sarcolemmal proteins including dystrophin, sarcoglycans, and dysferlin, (3) the sarcommeric proteins like myotilin, titin, and FHL-1, (4) the nuclear membrane proteins like emerin and lamin A/C, and (5) other miscellaneous proteins such as calpain 3 and TRIM32.

Given the number of proteins attributed to muscular dystrophy, it can be said to be a heterogeneous and variable pathogenesis. However, recent research has revealed important molecular mechanisms leading to muscle degeneration. We discuss three major issues. First, in the pathogenesis of dystrophinopathy, increased sarcolemmal fragility and increased Ca^{2+} influx have been observed. It is also revealed that TRPV2, a stretch-sensitive ion channel, plays a significant role in increasing Ca^{2+} influx. Second, dysferlin has been proved to be involved in the membrane repair system. In addition to the molecule dysferlin which works in a Ca^{2+}dependent manner, MG53 has been identified to play a significant role in membrane repair without Ca^{2+}. MG53 is also expected to be a novel therapeutic target molecule. Third, as a major underlying factor causing muscle damage in dystrophin-deficient skeletal muscle, decreased nNOS activity has been pointed. Dystrophin-deficient skeletal muscle is damaged as a consequence of disturbed vasodilation after muscle contraction. This is proved with *mdx* mice, where administration of a phosphodiesterase 5 inhibitor, a potent vasodilator, ameliorates muscle damage.

Although these findings at the protein level have great implications for the therapy of muscular dystrophy, clarifying the molecular mechanisms at the RNA level will be the key in developing novel therapeutic strategies. One of the new therapies for DMD could be the exon-skipping therapy where anti-sense agents are used to modify RNA splicing.

Am J Physiol Endocrinol Metab 300: E543–E553, 2011.
First published January 4, 2011; doi:10.1152/ajpendo.00430.2010.

Follistatin-derived peptide expression in muscle decreases adipose tissue mass and prevents hepatic steatosis

Masashi Nakatani,[1] Masahiro Kokubo,[2] Yutaka Ohsawa,[3] Yoshihide Sunada,[3] and Kunihiro Tsuchida[1]

[1]Division for Therapies against Intractable Diseases, Institute for Comprehensive Medical Science (ICMS), and [2]Joint Research Laboratories, Fujita Health University, Toyoake; and [3]Division of Neurology, Department of Internal Medicine, Kawasaki Medical School, Kurashiki, Japan

Submitted 20 July 2010; accepted in final form 3 January 2011

Nakatani M, Kokubo M, Ohsawa Y, Sunada Y, Tsuchida K. Follistatin-derived peptide expression in muscle decreases adipose tissue mass and prevents hepatic steatosis. *Am J Physiol Endocrinol Metab* 300: E543–E553, 2011. First published January 4, 2011; doi:10.1152/ajpendo.00430.2010.—Myostatin, a member of the transforming growth factor (TGF)-β superfamily, plays a potent inhibitory role in regulating skeletal muscle mass. Inhibition of myostatin by gene disruption, transgenic (Tg) expression of myostatin propeptide, or injection of propeptide or myostatin antibodies causes a widespread increase in skeletal muscle mass. Several peptides, in addition to myostatin propeptide and myostatin antibodies, can bind directly to and neutralize the activity of myostatin. These include follistatin and follistatin-related gene. Overexpression of follistatin or follistatin-related gene in mice increased the muscle mass as in myostatin knockout mice. Follistatin binds to myostatin but also binds to and inhibits other members of the TGF-β superfamily, notably activins. Therefore, follistatin regulates both myostatin and activins in vivo. We previously reported the development and characterization of several follistatin-derived peptides, including FS I-I (Nakatani M, Takehara Y, Sugino H, Matsumoto M, Hashimoto O, Hasegawa Y, Murakami T, Uezumi A, Takeda S, Noji S, Sunada Y, Tsuchida K. *FASEB J* 22: 477–487, 2008). FS I-I retained myostatin-inhibitory activity without affecting the bioactivity of activins. Here, we found that inhibition of myostatin increases skeletal muscle mass and decreases fat accumulation in FS I-I Tg mice. FS I-I Tg mice also showed decreased fat accumulation even on a control diet. Interestingly, the adipocytes in FS I-I Tg mice were much smaller than those of wild-type mice. Furthermore, FS I-I Tg mice were resistant to high-fat diet-induced obesity and hepatic steatosis and had lower hepatic fatty acid levels and altered fatty acid composition compared with control mice. FS I-I Tg mice have improved glucose tolerance when placed on a high-fat diet. These data indicate that inhibiting myostatin with a follistatin-derived peptide provides a novel therapeutic option to decrease adipocyte size, prevent obesity and hepatic steatosis, and improve glucose tolerance.

myostatin; adipocyte; fatty liver; glucose tolerance

THE TRANSFORMING GROWTH FACTOR (TGF)-β superfamily is one of the largest families of secreted growth and differentiation factors and plays important roles in regulating tissue development and homeostasis (37). Myostatin, a member of the TGF-β superfamily, acts as a negative regulator of muscle growth (19, 22). Mutations in the myostatin gene in cattle, sheep, dogs, and humans cause an increase in skeletal muscle mass, indicating conservation of its function in mammals (5, 8, 23, 26, 32, 33). Myostatin is expressed predominantly in skeletal muscle and at significantly lower levels in adipose tissue (22). Inhibition of myostatin causes an increase in skeletal muscle mass and ameliorates several models of muscular dystrophies. Therefore, myostatin inhibitors are a promising therapeutic target to treat muscular atrophy and muscular dystrophy (19, 29, 37).

The loss of myostatin by gene disruption prevents an age-related increase in adipose tissue mass and partially attenuates the obese and diabetic phenotypes (14, 24). The serum leptin concentration and adipose tissue leptin mRNA expression were lower in myostatin null mice than in wild-type mice (24). Inhibition of myostatin by transgenic (Tg) expression of myostatin propeptide was also reported to prevent diet-induced obesity (41, 42). Even when fed a high-fat diet (HFD), these mice exhibited normal insulin sensitivity, unlike wild-type mice (42). Furthermore, ΔACVR2B, a soluble extracellular form of the activin type IIB receptor, effectively decreased the adipose tissue mass (1). These results suggest that inhibition of myostatin signaling could be useful to prevent and/or treat obesity and diabetes.

There are several strategies to block the functions of myostatin, including myostatin propeptide, follistatin, follistatin-related gene (FLRG), follistatin domain-containing growth and differentiation factor-associated serum protein-1 (GASP-1), the potent myostatin inhibitor ΔACVR2B, neutralizing antibodies, and small chemical compounds that block receptor serine kinases (2, 15, 37, 38).

Follistatin was shown to bind to myostatin and inhibit its activity. However, follistatin inhibits other members of the TGF-β superfamily, including GDF11 and activin (11, 37, 38). Although GDF11 and myostatin show a high degree of sequence similarity at the amino acid level, GDF11 is unlikely to regulate skeletal muscle mass, because GDF11 controls skeleton and kidney development rather than regulating muscle mass (21). Like myostatin, activin regulates skeletal muscle mass (12). However, unlike myostatin, activin has many pleiotropic roles including ovarian and neuronal functions (30, 36). In our previous study, we reported the development and characterization of a myostatin inhibitor derived from follistatin, designated FS I-I. FS I-I is unable to neutralize activin but still binds to and inhibits myostatin (27). Tg expression of FS I-I using a skeletal muscle-specific promoter caused a widespread increase in skeletal muscle mass and ameliorated muscular dystrophy. In addition, muscle strength was recovered when the FS I-I Tg mice were crossed with *mdx* mice (27). In this study, we explored whether FS I-I Tg mice are resistant to diet-induced obesity and hepatic steatosis. We found that FS I-I Tg mice exhibited reduced fat accumulation even when fed a normal diet (NFD). Adipocytes were also much smaller than those of wild-type littermates. Furthermore, the FS I-I Tg mice

Address for reprint requests and other correspondence: K. Tsuchida, Division for Therapies against Intractable Diseases, Institute for Comprehensive Medical Science (ICMS), Fujita Health Univ., Toyoake, Aichi 470-1192, Japan (e-mail: tsuchida@fujita-hu.ac.jp).

were resistant to HFD-induced obesity and hepatic steatosis. The liver of HFD-fed FS I-I Tg mice showed significantly different fatty acid composition compared with that seen in the control mice. Our studies suggest that follistatin-derived myostatin inhibitors offer a therapeutic option for obesity, diabetes, and hepatic steatosis.

MATERIALS AND METHODS

Animals. The establishment of skeletal muscle-specific FS I-I Tg mice is described in our previous paper (27). In brief, *Eco*RI-*Sma*I fragment covering the whole coding sequence of FS I-I was subcloned into the MDAF2 vector containing the myosin light-chain promoter SV40 processing sites and MLC1/3 enhancer. *Cla*I fragment with 3.9 kb was microinjected to produce FS I-I transgenic mice (27). The transgene was expressed in skeletal muscles but not in cardiac muscle or adipose tissues. FS I-I Tg male mice and wild-type littermates were obtained from the offspring of FS I-I Tg mice mated with C57BL/6 mice. The genotypes were determined by PCR as previously described (27). The FS I-I Tg and littermate male mice were weaned at 4 wk of age and given free access to either a normal-fat (NFD; 5% kcal fat; CE-2; CLEA, Shizuoka, Japan) or a high-fat diet (HFD; 32% kcal fat, High Fat Diet 32, CLEA) from 4 to 13 wk. Food intake did not differ between the two genotypes on the HFD. Body weight was recorded every week. All mice were housed in cages with a constant temperature (22°C) and a 12:12-h light-dark cycle. All experiments were performed at the Laboratory Animal Center with approval from the Animal Research Committee at Fujita Health University.

Analysis of adipose tissue, skeletal muscle, and liver. Adipose tissues (retroperitoneal, epididymal, and inguinal fat pads), skeletal muscles [tibialis anterior (TA), extensor digitorum longus (EDL), quadriceps femoris (Qf), and soleus], and liver samples were obtained from mice at 13 or 20 wk of age. Adipose tissue and muscles were also obtained from NFD- and HFD-fed mice at *week 13*. The wet tissue weights were measured.

Histological analyses of adipose tissues and liver. The adipose tissues and livers either from FS I-I Tg mice or littermates were fixed in 4% paraformaldehyde (PFA), dehydrated in ethanol, embedded in paraffin, and sectioned at a thickness of 6 μm. The sections were then deparaffinized, rehydrated, and stained with hematoxylin and eosin (H&E). The area of adipocytes was determined in images stained with H&E. The area of 200 adipocytes per mouse was determined in five wild-type and five FSI-I Tg mice (1,000 adipocytes for each genotype), and the average cell area was determined. Morphometric analyses to measure adipocyte area and size were performed using WinROOF software (Mitani, Fukui, Japan).

Electron microscope analysis. Adipose tissue samples were fixed for 4 h with 2% PFA and 2.5% glutaraldehyde in phosphate-buffered saline (PBS) at room temperature. The specimens were then postfixed at room temperature for 1 h with 2% osmium tetroxide in Millonig's buffer containing 0.54% glucose and dehydrated through an ethanol gradient. For scanning electron microscopy, the dehydrated specimens were then immersed in *t*-butyl alcohol, dried using a freeze-drying device, coated with gold using an ion sputtering device (JEE-420T, JEOL), and examined under a scanning electron microscope (H7650; Hitachi, Tokyo, Japan). For transmission electron microscopy, specimens were immersed in QY-1 (Nisshin EM, Tokyo, Japan), embedded in epoxy resin (Epon812; Polyscience, Wako Pure Chemical Industries, Osaka, Japan), and cut into ultrathin sections. The sections were stained with uranyl acetate and lead citrate, followed by transmission electron microscopy at an accelerating voltage of 80 kV (JEM-1010TEM, JEOL). One hundred fifty mitochondria of epididymal adpipocytes each from three wild-type and FS I-I Tg mice were analyzed using WinROOF software.

Quantitative real-time PCR. The relative expressions of uncoupling protein-3 (UCP3), acetyl-CoA carboxylase-1 (ACC1), stearoyl-CoA desaturase-1 (SCD1), glucokinase (Gck), and phosphofructokinase (PFK) were determined by quantitative (q)PCR using a TAKARA Thermal Cycler Dice Real-Time System (Takara Bio, Shiga, Japan). Briefly, mRNA was isolated from liver and adipose tissues from FS I-I Tg mice and wild-type littermates by use of TRIzol (Invitrogen, Tokyo, Japan) with standard techniques. The isolated RNA was cleaned by DNaseI and purified using RNeasy Tissue kits (Qiagen, Tokyo, Japan). Reverse transcription was carried out with 500 ng of RNA using QuantiTect reverse transcription kits (Qiagen) according to the manufacturer's instructions.

We used Primer 3 software to design the primers for UCP3 (forward: 5′-CCGGTGGATGTGGTAAAGAC-3, reverse: 5′-AAGCTCCCAGACGCAGAAAG-3); ACC1 (forward: 5′-CCCATCCAAACAGAGGGAAC-3, reverse: 5-CTGACAAGGTGGCGTGAAG-3); SCD1 (forward: 5′-CAAGCTGGAGTACGTCTGGA-3′, reverse: 5′-CAGAGCGCTGGTCATGTAGT-3′); Gck (forward: 5′-TGGGCTTCACCTTCTCCTTC-3′, reverse: 5′-CGATGTTGTTCCCTTCTGCT-3′); and PFK (forward: 5′-GAAGCCAATCACCTCAGAAGAC-3′, reverse: 5′-TTCCACACCCATCCTGCT-3′). Each well of the 96-well reaction plate contained a total volume of 25 μl. cDNA (0.5 μl) solution was combined with each of forward and reverse primers (10 μM), distilled water, and SYBR Premix Ex Taq (Takara Bio). All reactions were performed in triplicate. The relative amounts of RNAs were calculated using the comparative C_T method. We used hepatic glyceraldehyde-3-phosphate dehydrogenase (GAPDH) and adipose tissue 36B4 as controls. Significant differences between the wild-type and FS I-I Tg mice were analyzed by Student's *t*-test.

Western blotting. Adipose tissues (epididymal and inguinal fat pads), skeletal muscle (Qf), and liver were dissected from wild-type and FSI-I Tg mice. Samples were homogenized in a buffer containing 50 mM Tris·HCl, pH 7.5, 150 mM NaCl, 5 mM NaF, 1% Nonidet P-40, 5 mM β-glycerophosphate, 1 mM phenylmethylsulfonyl fluoride, 4 μg/ml leupeptin, and 1 μg/ml aprotinin and centrifuged at 15,000 rpm for 10 min at 4°C, and the lipid-free lysates were collected. Aliquots of the lysates containing 30 μg of protein or serum containing 60 μg of protein were separated by sodium dodecyl sulfate-polyacrylamide gel electrophoresis and transferred onto polyvinylidene difluoride membranes. The membrane was blocked in 5% skim milk for 1 h at room temperature. The membranes were then probed with anti-cytochrome *c*, phosphorylated Smad 3, or Smad 3 (Cell Signaling Technology, Beverly, MA) at 4°C overnight (1:1,000 dilution), followed by incubation with horseradish peroxidase-conjugated secondary antibodies and chemiluminescence reactions by ECL plus (GE Healthcare, Tokyo, Japan). As a loading control, antibodies to tubulin or actin (Cell Signaling Technology, Beverly, MA) were used. Detection of FS I-I or follistatin by Western blotting was performed using rabbit polyclonal antibodies (ABPIII) raised against follistatin domain I of follistatin (31). Images of the developed immunoblots were captured using a cooled CCD camera system (Light-Capture; ATTO, Tokyo, Japan).

Measurement of serum parameters and triglycerides. Wild-type and FS I-I Tg mice ($n = 4–6$ per group) fed the NFD or HFD from *weeks 4* to *13* of age were fasted overnight at *week 13* for 16 h before blood sampling. The triglyceride, nonesterified fatty acid (NEFA), cholesterol, fasting glucose, insulin, leptin, and adiponectin concentrations were measured in serum samples prepared from whole blood collected from the retroorbital venous plexus of anesthetized mice. Plasma, total cholesterol, and NEFA were measured using enzymatic assays (triglyceride E, cholesterol E, and NEFA tests, respectively; Wako Pure Chemical Industries, Osaka, Japan). Plasma leptin, adiponectin, and insulin levels were measured using enzyme-linked immunoassays from Morinaga (Kanagawa, Japan), R&D systems (Gunma, Japan), and Otsuka (Tokyo, Japan), respectively. Triglycerides from liver and skeletal muscle were extracted with chloroform-methanol (2:1, vol/vol), centrifuged twice to remove debris, dried, and resuspended in 2-propanol containing 10% Triton X-100 (17). Triglyceride contents were enzymatically measured using a triglyceride E test. Mouse preadipocyte 3T3-L1 cells and human hepatocyte Hep

G2 cells were grown in Dulbecco's modified Eagle's medium (DMEM) supplemented with 10% fetal calf serum. Cells (1×10^5)/12-well plates of differentiating 3T3-L1 cells were stimulated with either 80 ng/ml FS I-I or 40 ng/ml myostatin (R&D systems) for 3 days. Hep G2 cells treated with 3 mg/ml glucose, 10 μg/ml insulin, and either 80 ng/ml FS I-I or 40 ng/ml myostatin for 3 days. Cellular triglycerides were extracted and measured as described above. All assays were performed according to the manufacturer's protocol.

Glucose tolerance test. Glucose tolerance tests were performed in six to eight mice per group at 13 wk of age after being fed the NFD or HFD for 9 wk. The mice were fasted overnight and then received an intraperitoneal injection of 10% dextrose (1 g/kg body wt). Blood was collected from the tail at 0, 15, 30, 60, and 120 min after dextrose injection, and blood glucose was measured using an Accu-Check glucose monitor (Roche Diagnostic, Indianapolis, IN).

Insulin tolerance test. Insulin tolerance tests were performed in five mice per group at 13 wk of age after being fed the HFD for 9 wk. The mice were starved for 16 h and received an intraperitoneal injection of human insulin (0.75 U/kg body wt; Sigma-Aldrich Japan). Blood glucose was measured at 0, 30, 60, and 90 min after injection using an Accu-Check glucose monitor (24).

Measurement of hepatic fatty acid content. Approximately 100 mg of liver tissue was obtained from wild-type and FS I-I Tg mice fed the NFD or HFD for 9 wk ($n = 6$ per group). Lipids were extracted using the Bligh-Dyer chloroform-methanol method (4). The extracted lipids were dissolved in 1 ml of chloroform and subjected to methanolysis-gas chromatographic analysis (3). Methyl stearate was used to generate a standard curve for quantitation. The determinations were repeated at least twice, and essentially the same results were obtained.

Metabolic rate analysis. Oxygen consumption was measured with an indirect calorimetric metabolism measuring system (model MK-5000RQ, Muromachikikai) (17). Each mouse was kept in a sealed chamber with an air flow of 0.6 l/min for 2 h during the light cycle. Air was sampled every 3 min, and the consumed oxygen concentration ($\dot{V}O_2$) was calculated (24). Five mice each for wild-type and FS I-I Tg mice fed NMD were analyzed.

Statistical analysis. Results are presented as means ± SD. Statistical significance was assessed by Student's *t*-tests. Differences between groups were considered statistically significant at $P < 0.05$. *P* values are presented in figure and table legends.

RESULTS

Decreased fat accumulation in FS I-I tg mice. We previously reported (27) that FS I-I Tg mice show a marked increase in skeletal muscle mass compared with wild-type mice when fed a NFD. Intriguingly, even with a NFD, FS I-I Tg mice showed age-dependent decreased fat accumulation. Although there was no difference in individual fat pad weights between wild-type and FS I-I Tg mice at 13 wk of age (data not shown), there was a significant difference at 20 wk of age. For example, at 20 wk of age, the weight of the epididymal fat pad was 60% lower in FS I-I Tg mice than in wild-type mice (Fig. 1*A*). Furthermore, the weights of the inguinal and retroperitoneal fat pads of FS I-I Tg mice were 33 and 67% lower, respectively, in FS I-I Tg mice than in wild-type mice. Therefore, we quantified the adipocyte size histologically using H&E staining (Fig. 1*B*)

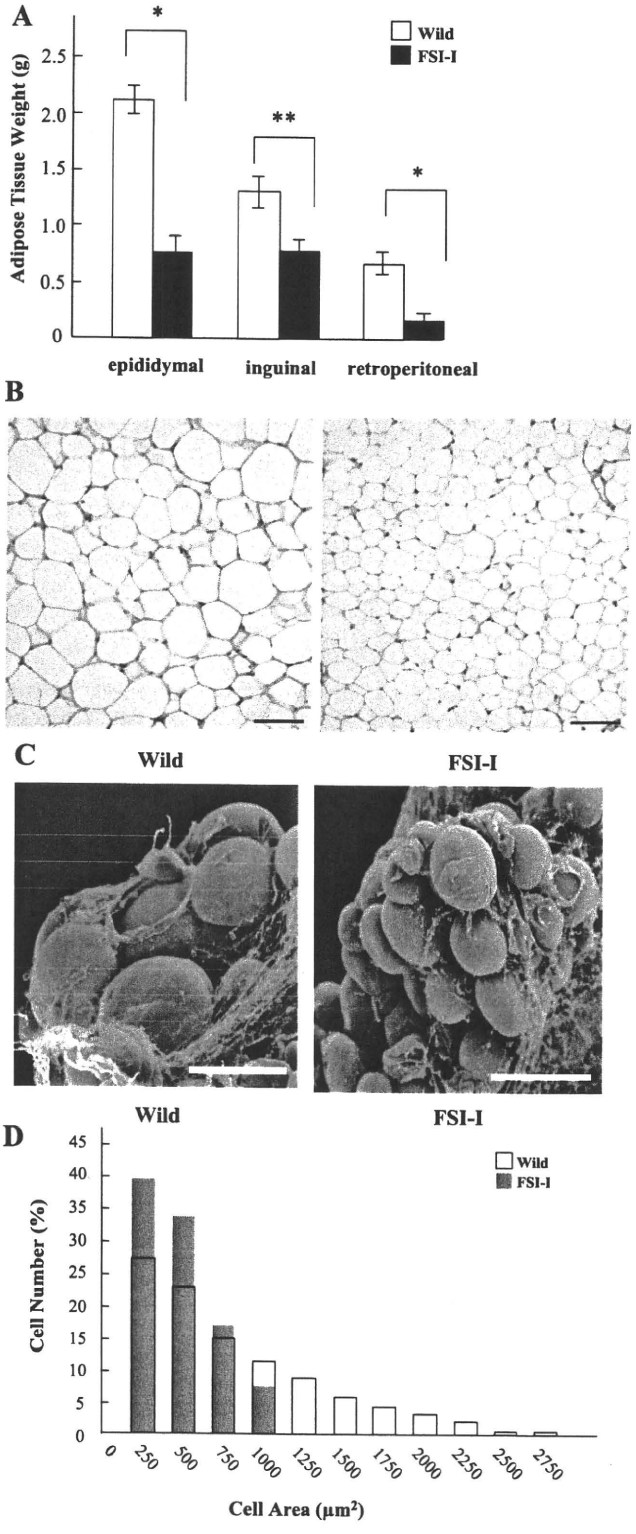

Fig. 1. *A*: adipose tissue weights (g) of 20-wk-old male wild-type and transgenic (Tg) mice with a myostatin inhibitor derived from follistatin [follistatin (FS)-derived peptide (FS I-I)] fed a control diet. Epididymal, inguinal, and retroperitoneal fat pads from 5 mice each from wild-type and FSI-I Tg mice were dissected and weighed. $^*P < 0.005$ and $^{**}P < 0.03$, Student's *t*-test. *B*: histological analysis of adipose tissues. Epididymal fat pads from 20-wk-old wild-type and FS I-I Tg mice were sectioned and stained with H&E. Scale bar, 100 μm. *C*: scanning electron microscopy of epididymal fat pads. 20-wk-old wild-type (*left*) and FS I-I Tg mice (*right*) were analyzed. Scale bar, 120 μm. *D*: distribution of epididymal adipocyte area in 20-wk-old wild-type and FS I-I Tg mice; 200 adipocytes were counted per mouse (5 mice per group). The percentage of adipocytes with indicated areas per total adipocytes was calculated and plotted. The mean adipocyte area was smaller in FS I-I Tg mice (717.4 ± 579.1 μm^2) than in wild-type mice (436.8 ± 309.1 μm^2).

and by scanning electron microscopy (Fig. 1*C*). Both techniques confirmed that adipocyte size was smaller in FS I-I Tg mice than in wild-type mice. Therefore, we determined the mean adipocyte area. Quantification of the area of individual adipocytes is shown in Fig. 1*D*. At *week 20* of age, the mean adipocyte area was smaller in FS I-I Tg mice than in wild-type mice (436.8 ± 309.1 vs. 717.4 ± 579.1 μm^2, respectively; Fig. 1*D*). These results indicate that FS

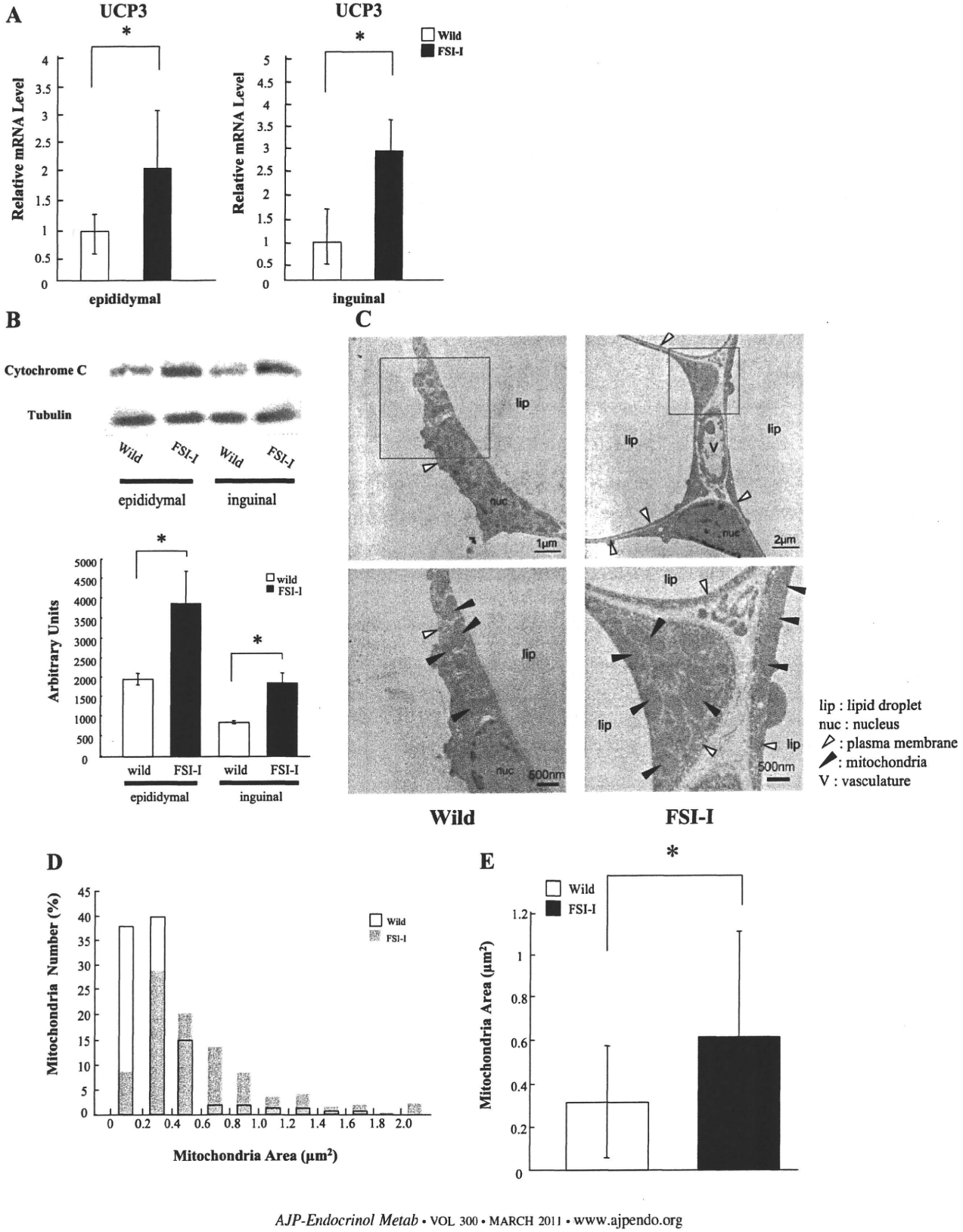

I-I Tg mice showed less fat accumulation than wild-type mice when fed a NFD.

Changes in expression of metabolic molecules in FS I-I Tg mice. We examined the expression levels of mRNAs encoding the UCPs, proteins expressed on the inner membrane of the mitochondria that uncouple the proton gradient from ATP synthesis and are implicated in thermogenesis (7). The expression levels of UCP3 in epididymal and inguinal adipose tissues were increased two- and threefold, respectively, in FS I-I Tg mice compared with wild-type mice (Fig. 2*A*). However, the expression levels of UCP1 and UCP2 mRNAs in adipose tissues in FS I-I Tg mice and wild-type mice were comparable (data not shown).

We next quantified the abundance of mitochondria in adipose tissues by using the mitochondria marker cytochrome *c* (Fig. 2*B*). Consistent with the increase in UCP3 mRNA, the protein expression of cytochrome *c* was increased in the epididymal and inguinal fat pads in FS I-I Tg mice compared with wild-type mice (Fig. 2*B*). In skeletal muscle, cytochrome expression did not change (Suppl. Fig. S1; supplementary materials are found with the online version of this paper on the Journal website). We also determined mitochondria size by transmission electron microscopy (Figs. 2, *C* and *D*, and S2), which revealed that both the number and size of mitochondria in adipocytes were increased in FS I-I Tg mice compared with wild-type mice. These results raise the interesting possibility that FS I-I Tg mice exhibit increased energy metabolism and/or energy partitioning between adipose tissue and skeletal muscle.

Expression of FS I-I and altered Smad 3 phosphorylation in FS I-I Tg mice. To ascertain that FS I-I expression is restricted in skeletal muscle, we performed Western blotting using skeletal muscle, liver, adipose tissues and serum from wild-type and FS I-I Tg mice. As shown in Fig. 3*A*, FS I-I protein was expressed in skeletal muscle, but was not detected in either liver or adipose tissues. In serum, follistatin was detected, whereas FS I-I was hardly detectable. Next, we studied the phosphorylation of Smad 3 protein by immunoblotting. As shown in Fig. 3*B*, Smad 3 phosphorylation in skeletal muscle from FS I-I Tg mice was significantly reduced compared with that from control mice. In other tissues such as liver and adipose tissues, Smad 3 phosphorylation was either undetectable or unchanged.

FS I-I Tg mice are resistant to HFD-induced obesity. We previously reported that NFD-fed FS I-I Tg mice exhibited greater weight gain than wild-type mice between 6 and 15 wk of age, even though food intakes were comparable (27). Here, the FS I-I Tg and wild-type mice were fed a HFD from *weeks 4* to *13* of age to induce obesity. Interestingly, weight gain did not differ between FS I-I Tg and wild-type mice (Fig. 4*A*). However, the weight of adipose tissue depots was lower in FS I-I Tg mice than in wild-type mice, being 25.0 and 34.3% lower for the inguinal and retroperitoneal fat pads, respectively (Fig. 4*B*). By contrast, FS I-I Tg mice exhibited increased muscle weight, as the TA, EDL, Qf, and soleus muscles were 43, 45, 21, and 27% higher in FS I-I Tg mice than in wild-type mice (Fig. 4*C*). Thus, the absence of a difference in body weight gain between wild-type mice and FS I-I Tg mice fed the HFD was attributed to changes of adipose tissue, muscle, and liver weights in FS I-I Tg mice (see Figs. 4, *B* and *C*, and 5*B*).

We next measured serum parameters, including triglyceride, NEFA, total cholesterol, insulin, leptin, and adiponectin levels

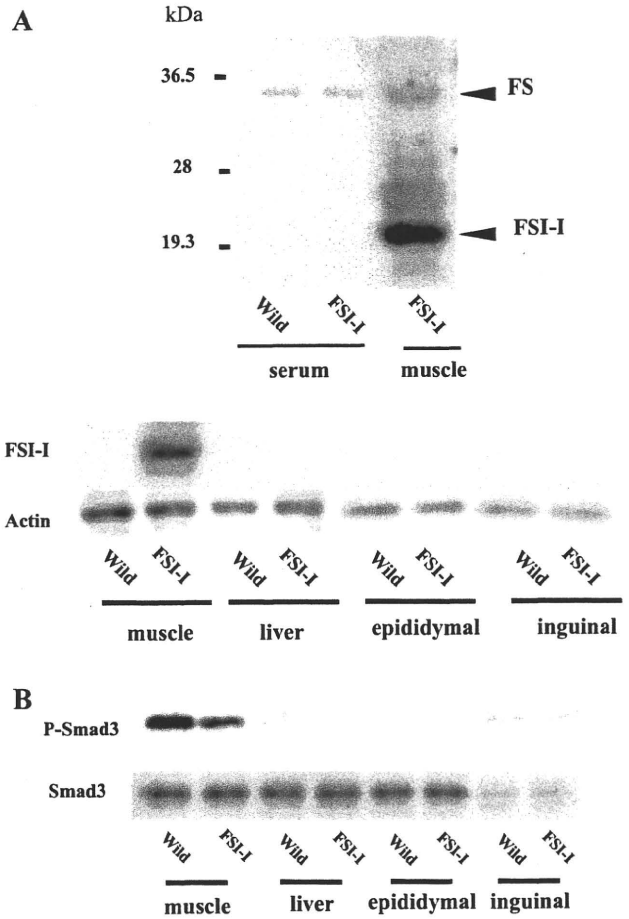

Fig. 3. *A*: detection of FS and FS I-I in serum, femoris skeletal muscle (Qf), liver, and fats. FS is detected as 33-kDa protein in serum, whereas FS I-I is not detectable in serum in FS I-I Tg mice (*top*). FS I-I is detected in skeletal muscle but not in liver or fats (*bottom*). *B*: detection of phosphorylated Smad3 in skeletal muscle, liver, and epididymal and inguinal fats. In quadriceps skeletal muscle (Qf) of FS I-I Tg mice, phosphorylated Smad 3 is reduced compared with that of wild-type mice. Smad 3 antibody was used as a loading control. In other tissues, phosphorylation of Smad 3 is either undetectable or unchanged.

Fig. 2. *A*: relative mRNA expression of UCP3 in epididymal and inguinal adipose tissues in wild-type and FS I-I Tg mice. Adipose tissues from 5 mice each for wild-type and FS I-I Tg mice were used and quantitated. UCP3 mRNA expression levels were quantified by RT-PCR. $*P < 0.05$, Student's *t*-test. *B*: protein expression of cytochrome *c* in epididymal and inguinal fat pads from wild-type and FS I-I Tg mice. Cytochrome *c* was detected at 14 kDa. Tubulin expression was used as a loading control (*top*). Adipose tissues from 3 mice each for wild-type and FS I-I Tg mice were used and quantitated. $*P < 0.02$, Student's *t*-test (*bottom*). *C*: transmission electron microscopy of epididymal adipose tissues from 20-wk-old wild-type and FS I-I Tg mice. Higher magnification views of indicated regions (squares) at *top* are shown at *bottom*. Scale bars, 1 μm in *top left*, 2 μm in *top right*, and 500 nm in *bottom*. Lip, lipid droplet; nuc, nucleus; white arrowheads, plasma membranes; black arrowheads, mitochondria; V, vasculature. *D*: analysis of mitochondria size and number from wild-type and FS I-I Tg mice. One hundred fifty mitochondria of epididymal adipocytes each from 3 wild-type and FS I-I Tg mice were analyzed and plotted. *E*: mean mitochondria areas of wild-type and FS I-I Tg mice. $*P < 0.001$, Student's *t*-test.

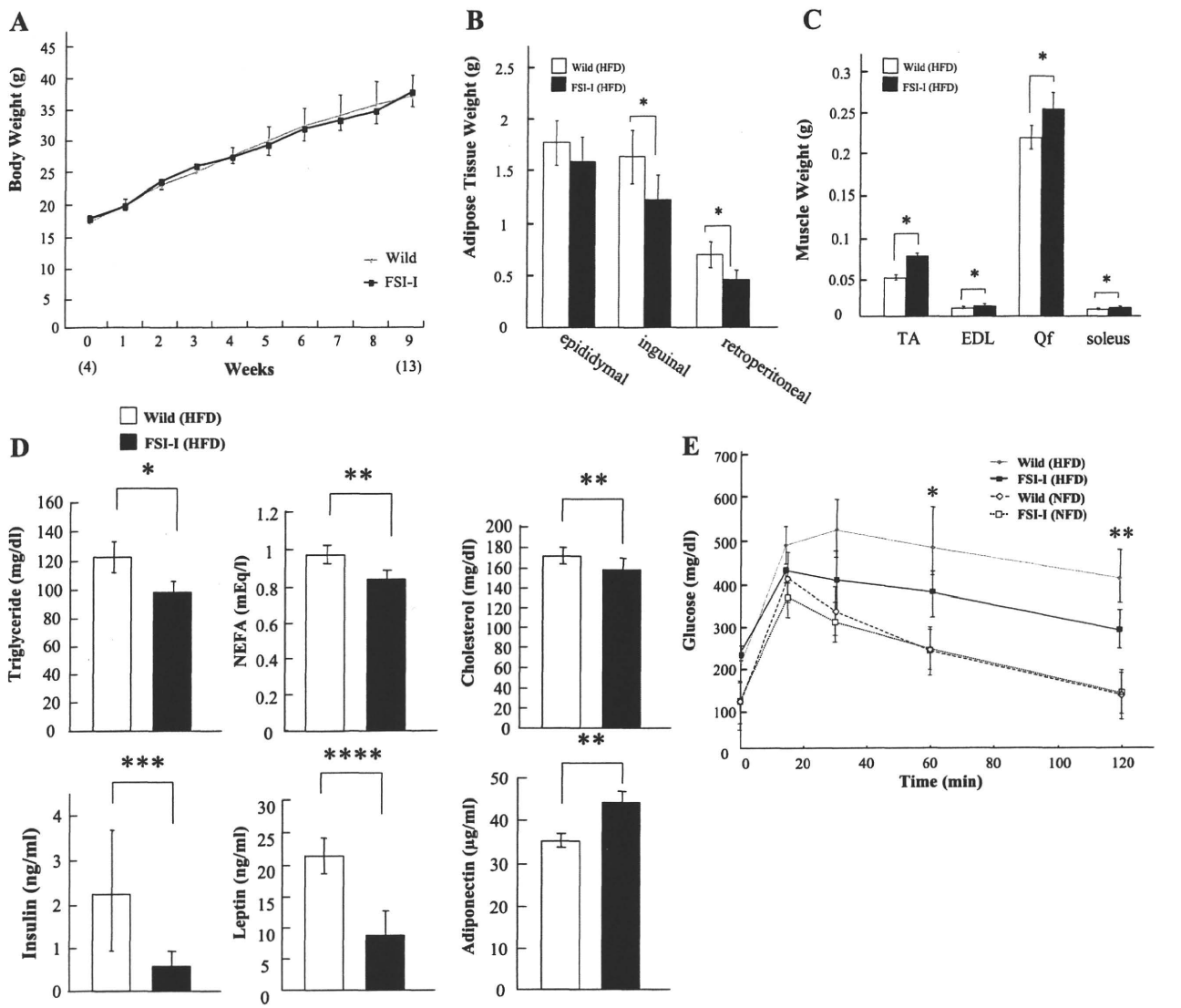

Fig. 4. *A*: body weights (g) of wild-type and FS I-I Tg mice fed a high-fat diet (HFD) from 4 to 13 wk of age; $n = 5$ mice per group. *B*: weight of epididymal, inguinal, and retroperitoneal fat pads of wild-type and FS I-I Tg mice fed HFD from 4 to 13 wk of age. $*P < 0.05$, Student's *t*-test; $n = 5$–6 mice per group. *C*: weights of the tibialis anterior (TA), extensor digitorum longus (EDL), quadriceps femoris (QF), and soleus muscles from wild-type and FS I-I Tg mice fed a HFD from 4 to 13 wk of age. $*P < 0.005$, Student's *t*-test; $n = 5$ mice per group. *D*: triglycerides, NEFA, cholesterol, insulin, leptin, and adiponectin levels in wild-type and FS I-I Tg mice fed HFD from 4 to 13 wk of age. $*P < 0.0005$, $**P < 0.003$, $***P < 0.05$, $****P < 0.007$, Student's *t*-test; $n = 4$–6 mice per group. *E*: glucose tolerance test in wild-type and FS I-I Tg mice fed either normal diet (NFD) or HFD from 4 to 13 wk of age. Blood glucose was measured at 0, 15, 30, 60, and 120 min after glucose (dextrose) injection; $n = 6$–8 mice per group. $*P < 0.05$ and $**P < 0.01$, Student's *t*-test.

in FS I-I Tg and wild-type mice (Fig. 4*D*). Of note, triglyceride, NEFA, cholesterol, and leptin levels were lower in FS I-I Tg mice by 19.7, 13.6, 7.7, and 58.4%, respectively, compared with wild-type mice (Fig. 4*B* and Table 1). However, the serum adiponectin levels were 25.7% higher in FS I-I Tg mice than in wild-type mice when fed the HFD. By contrast, there were no significant differences in triglyceride, NEFA, cholesterol, leptin, and adiponectin levels between NFD-fed FS I-I Tg and wild-type mice (Table 1).

Defects in glucose homeostasis are important factors involved in the development of obesity. Therefore, we measured whole body glucose tolerance in FS I-I and wild-type mice fed the NFD or the HFD. Although there were no differences between NFD-fed FS I-I and wild-type mice, the glucose level tended to be lower in HFD-fed FS I-I Tg mice than in HFD-fed wild-type mice (Fig. 4*E*). These results indicate that the response to diet-induced obesity differs between FS I-I Tg and wild-type mice. In the NFD condition, no difference was observed in insulin tolerance (data not shown). However, in the HFD condition, FS I-I Tg mice exhibited better insulin tolerance than wild-type mice (Fig. S3).

FS I-I Tg mice are resistant to HFD-induced hepatic steatosis. As expected, the HFD increased hepatocyte lipid content and induced hepatic steatosis in wild-type mice. However, hepatic steatosis was not observed in HFD-fed FS I-I Tg mice (Fig. 5*A*). The liver from FS I-I Tg mice was histologically normal, even when these mice were fed the HFD, and showed significantly less lipid accumulation than HFD-fed

Table 1. *Serum metabolic parameters in wild-type and FS I-I Tg mice fed NFD or HFD*

	NFD		HFD	
Diet Treatment Genotype	Wild Type	FSI-I Tg	Wild Type	FSI-I Tg
Triglyceride, mg/dl	108.5 ± 10.3	101.1 ± 7.5	122.8 ± 10.6	98.6 ± 7.5[a]
NEFA, mEq/l	0.83 ± 0.05	0.73 ± 0.09	0.97 ± 0.05	0.84 ± 0.04[b1]
Cholesterol, mg/dl	91.8 ± 4.9	81.2 ± 1.7	170.8 ± 7.7	157.6 ± 10.7[b2]
Fasting glucose, mg/dl	101.2 ± 16.2	107.8 ± 14.7	208.0 ± 2.0	208.0 ± 6.6
Insulin, ng/ml	0.91 ± 0.13	0.51 ± 0.12[b4]	2.16 ± 1.56	0.58 ± 0.34[c]
Leptin, ng/ml	4.00 ± 0.41	3.88 ± 0.14	21.35 ± 2.74	8.90 ± 3.88[d]
Adiponectin, μg/ml	21.0 ± 1.2	20.4 ± 1.3	35.1 ± 1.6	44.0 ± 2.4[b3]

Values are means ± SD; $n = 4-6$ mice per group. NFD, normal fat diet; HFD, high-fat diet; FSI I-I Tg, follistatin-derived peptide transgenic. a, b1–b3, c, and d, vs. wild-type mice (HFD); b4, vs. wild-type mice (NFD). [a]$P < 0.0005$; [b1–b4]$P < 0.003$; [c]$P < 0.05$; [d]$P < 0.007$ (Student's *t*-test).

wild-type mice (Fig. 5*A*). In addition, hepatic steatosis did not develop even in aged mice in FS I-I Tg mice (data not shown). The weight of the liver in HFD-fed FS I-I Tg mice was 13% less than that of wild-type mice (Fig. 5, *A* and *B*). The lower liver weight in FS I-I mice was attributed to reduced hepatocyte triglyceride accumulation in these mice compared with wild-type mice (Fig. 5*C*). Triglyceride contents in skeletal muscle were not significantly different between FS I-I mice and wild-type mice fed the HFD in our experimental condition (data not shown).

We next performed qPCR to determine the mRNA expression of genes related to fatty acid synthesis, including SCD1, which is required for the biosynthesis of monounsaturated fatty acids such as oleic acid and plays a key role in the hepatic synthesis of triglycerides (25). The hepatic SCD1 mRNA expression levels were 20% lower in HFD-fed FS I-I Tg mice than in wild-type mice (Fig. 6*A*). By contrast, the mRNA expression of ACC1 mRNA did not differ between FS I-I Tg and wild-type mice. We also measured the mRNA expression levels of Gck and PFK, two enzymes that regulate the glycolytic pathway. The expression levels of both genes were increased in FS I-I Tg mice compared with wild-type mice, 1.8-fold for GcK and 2-fold for PFK (Fig. 6*A*).

We measured hepatic fatty acid content in FS I-I Tg and wild-type mice. Interestingly, in HFD-fed mice, the fatty acid content and the ratio of fatty acids differed between the FS I-I Tg and wild-type mice. For example, the livers from HFD-fed FS I-I Tg mice showed an increased stearyl acid (C18:0) ratio and decreased oleic acid (C18:1) ratio to the total fatty acid content (Fig. 6*B* and Table 2). The absolute content of oleic acid (C18:1) and palmitoleic acid (C16:1) did not increase in FS I-I Tg mice compared with wild-type mice (Table 2). This finding is consistent with the decreased mRNA level of SCD1. Taken together, these results indicate that FS I-I Tg mice were resistant to hepatic steatosis induced by HFD and had reduced monounsaturated fatty acid content, particularly oleic acid (C18:1) and palmitoleic acid (C16:1).

DISCUSSION

Inhibition of myostatin is useful for various muscular diseases, including muscular dystrophies, muscular atrophy, cachexia induced by cancer, and sarcopenia (19, 34, 38). Furthermore, myostatin-null mice and myostatin propeptide-overexpressing Tg mice were used to study the effects of myostatin inhibition on obesity (10, 14, 24, 41, 42). These studies revealed that the inhibition of myostatin decreased adipose tissue accumulation and improved diet-induced obesity and genetic diabetes/obesity. The loss of myostatin in genetically obese mice partially suppressed adipose tissue accumulation and improved glucose metabolism (24). Meanwhile, upon high-fat feeding, the myostatin propeptide Tg mice showed favorable fat utilization and beneficial interactions between skeletal muscle and adipose tissues compared with control mice (42). Recent studies have suggested that inhibiting myostatin in muscle but not in adipose tissues is responsible for the decreased fat mass and improved insulin sensitivity (13). Indeed, inhibition of myostatin signaling in adipose tissue by ΔACVR2B had no effect on body composition, weight gain, or insulin tolerance either on NFD or on HFD. By contrast, inhibition of myostatin by ΔACVR2B in skeletal muscle resulted in increased lean mass, decreased fat mass, and improved glucose metabolism in mice fed an NFD or an HFD (13).

In our previous study, we reported the development and characterization of a novel myostatin inhibitor derived from follistatin, designated FS I-I. Although FS I-I showed significantly weaker inhibitory effects on activin, FS I-I retained its inhibitory effect on myostatin. In FS I-I Tg mice, inhibition of myostatin activity by FS I-I increased skeletal muscle mass and strength (27). Cardiac weight did not increase in FS I-I mice (Fig. S5). In this study, we have further demonstrated that Tg expression of the myostatin inhibitor FS I-I also has an anti-obesity effect and improved glucose tolerance and prevents hepatic steatosis induced by HFD.

Various strategies can be exploited to inhibit myostatin, including neutralizing monoclonal myostatin antibodies, myostatin propeptide and ΔACVR2B (19). The neutralizing antibody is effective, but it can cause anti-idiotype immunity after in vivo administration. The myostatin propeptide is susceptible to proteolytic cleavage by members of the bone morphogenetic protein (BMP)-1/tolloid family of metalloproteinases, impairing its ability to inhibit myostatin (40). Purified follistatin has several cleaved isoforms; the COOH-terminal region is susceptible to proteinase cleavage, although the cleaved follistatin molecules can still inhibit activin and myostatin (36). FS I-I comprises the NH_2-terminal region and two consecutive follistatin domain I regions. Therefore, FS I-I lacks the native follistatin COOH-terminal region, which is susceptible to protease cleavage. Furthermore, follistatin is a naturally occurring peptide and may cause fewer immune responses than exogenous antibodies. Therefore, among myostatin inhibitors, FS I-I offers some advantages over monoclonal antibodies and myostatin propeptide.

Adipocytes in FS I-I Tg mice contained fewer lipids than wild-type mice when they were fed a standard diet. Therefore,

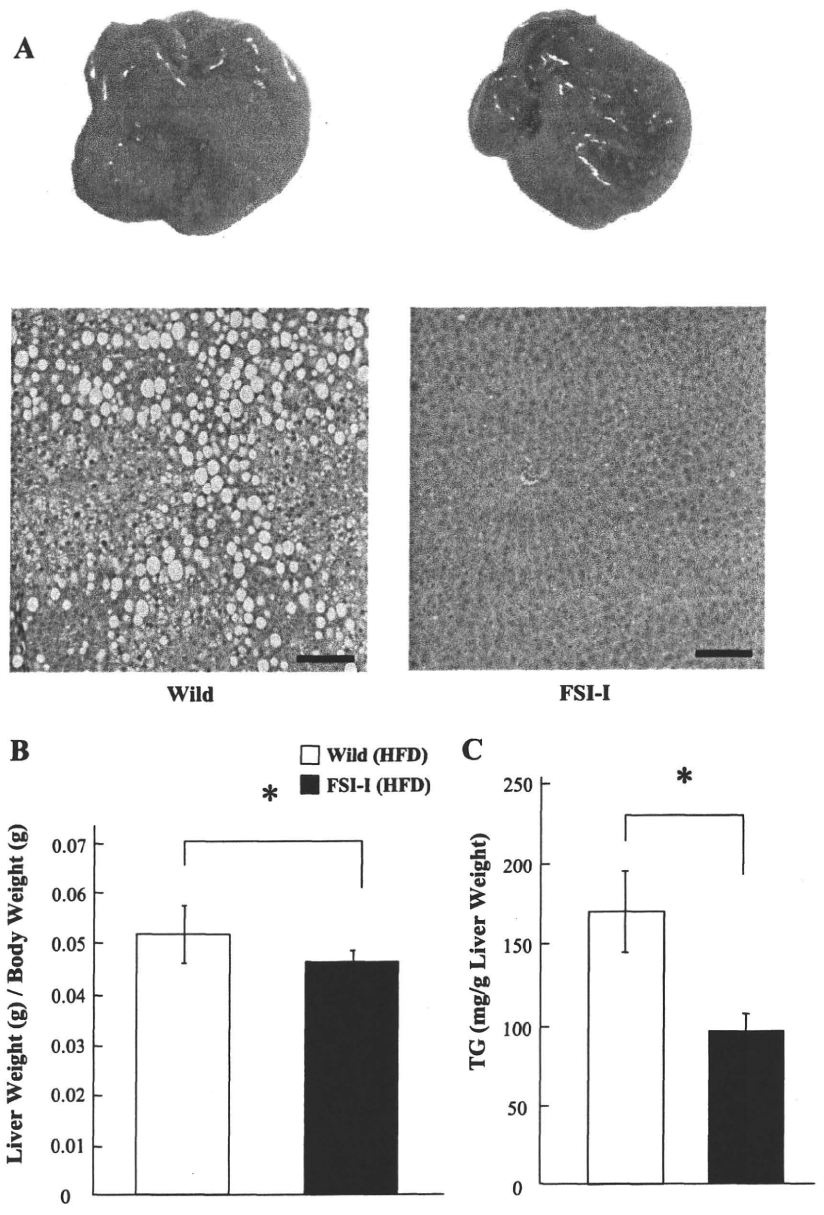

Fig. 5. *A*: morphology of liver samples from 13-wk-old wild-type and FS I-I Tg fed HFD. Liver sections were analyzed with H&E staining (*bottom*). Scale bar, 100 μm. *B*: relative liver weight (g) to body weight (g) of wild-type and FS I-I Tg mice fed HFD from 4 to 13 wk of age; $n = 6$ mice per group. $^*P < 0.01$, Student's *t*-test. *C*: hepatic triglyceride (TG) content in wild-type and FS I-I Tg mice fed HFD from 4 to 13 wk of age; $n = 5$ mice per group. $^*P < 0.0005$, Student's *t*-test.

mean adipocyte size was smaller in FS I-I Tg mice than in wild-type mice (Fig. 1, *B–D*). By contrast, fat mass was normal in myostatin propeptide Tg mice fed a standard diet (42). During HFD feeding, myostatin knockout mice gained fat mass, whereas muscle weight was unaffected by the HFD. By contrast, in FS I-I Tg mice, the skeletal muscle mass was still increased, albeit blunted compared with control mice (27, 42). The differences in the increases of fat and skeletal muscle mass in these models might be due to how much endogenous active myostatin is present in vivo.

We examined the expression levels of mRNAs encoding UCPs. The adipose tissue in FS I-I Tg mice showed upregulation of UCP3 mRNA expression levels (Fig. 2*A*) but not UCP1 or UCP2 compared with wild-type mice (data not shown). While UCP2 shows rather ubiquitous expression, UCP1 is specifically expressed in brown adipocytes and UCP3 is specifically expressed in skeletal muscle, brown adipose tissues, and heart (6, 18). Upregulation of UCP3 mRNA expression levels in FS I-I Tg mice was thought to increase energy expenditure. In addition, we observed adipose tissue by transmission electron microscopy (Fig. 2*C*). We found that the adipocytes in FS I-I Tg mice contained increased numbers of mitochondria. The mitochondria in FS I-I Tg adipocyte contained mitochondrial cristae, suggesting that they had normal mitochondrial function. To our knowledge, this is the first report demonstrating that myostatin inhibition causes an apparent increase in mitochondria abundance. The biogenesis of mitochondria requires coordinated protein synthesis and as-

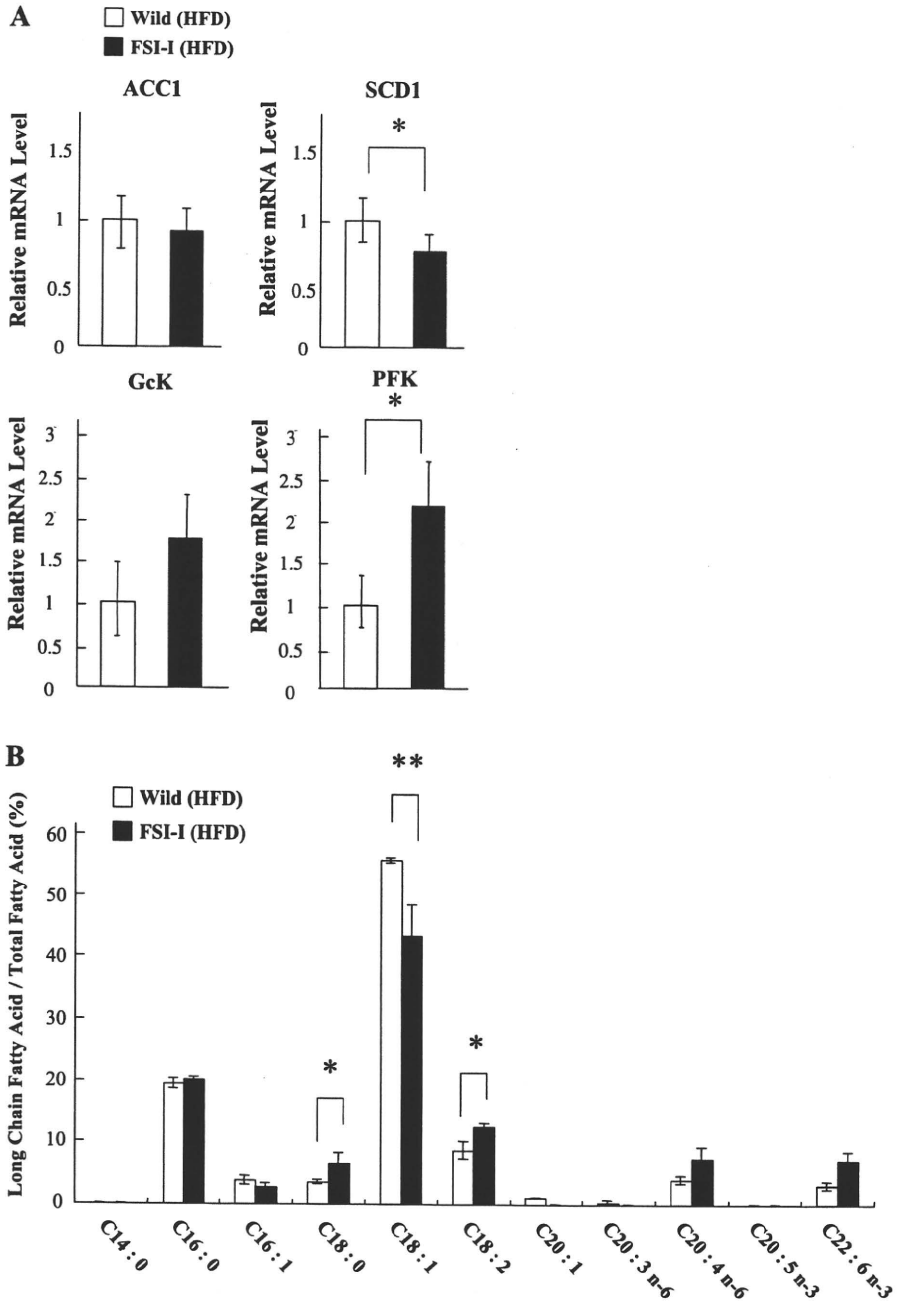

Fig. 6. *A*: relative hepatic mRNA expression levels of ACC1, SCD1, Gck, and PFK were measured by qPCR in wild-type and FS I-I Tg mice fed HFD; $n = 5$ mice per group. $^*P < 0.05$, Student's *t*-test. *B*: ratio of long-chain fatty acids to total fatty acids in liver of wild-type and FS I-I Tg mice fed HFD; $n = 6$ mice per group. $^*P < 0.05$ and $^{**}P < 0.03$, Student's *t*-test.

sembly from both the nuclear and mitochondrial genomes. Mitochondrial abundance can be modulated in response to physical activity, metabolic demands, and nutrition (16). PPARγ ligands increase mitochondrial biogenesis in white adipose tissue, and the PPARγ coactivator-1 (PGC-1) family is well characterized as a pivotal transcriptional coactivator for mitochondrial biogenesis (16). Although the mechanism of how mitochondria number and size are increased in adipocytes of FS I-I Tg mice remains to be determined, one possible mechanism may be upregulation of the PGC-1-dependent transcription cascade in white adipose tissues. Alternatively, it is also possible that the rate of mitochondrial turnover could be changed in white adipocytes of FS I-I Tg mice. Energy expenditure in FS I-I Tg mice was influenced by increased muscle mass, whereas adipose tissue is involved in energy storage. Therefore, changes in mitochondria abundance in adipocytes could modulate whole body energy expenditure and storage.

The insulin level in HFD-fed FS I-I Tg mice was lower than that in control mice (Fig. 4*D*), but glucose tolerance was better in HFD-fed FS I-I Tg mice than in HFD-fed wild-type mice. FS I-I is expressed under a skeletal muscle-specific myosin light-chain promoter and shows a widespread increase in muscle mass. The expression of FSI-I is restricted to skeletal muscles and is not detected in adipose tissues, liver, or serum (Fig. 3*A*). The circulating level of FSI-I in serum is under the detection limit and low compared with that of follistatin.

Table 2. *Hepatic fatty acid in wild-type and FS I-I Tg mice fed NFD or HFD*

Diet Treatment	NFD		HFD	
Genotype	Wild Type	FSI-I Tg	Wild Type	FSI-I Tg
C14:0	ND	ND	ND	ND
C16:0	13.1 ± 7.2	10.5 ± 4.9	20.2 ± 4.9	10.5 ± 2.8[a1]
C16:1	2.1 ± 1.7	1.3 ± 0.9	3.8 ± 1.1	1.5 ± 0.6[a2]
C18:0	3.0 ± 0.4	3.3 ± 1.0	3.5 ± 0.4	3.2 ± 0.1
C18:1	27.1 ± 22.1	21.4 ± 17.3	57.8 ± 12.0	23.1 ± 9.4[b]
C18:2	7.2 ± 2.1	6.7 ± 2.0	8.9 ± 2.7	6.4 ± 1.5
C20:1	0.3 ± 0.5	ND	1.1 ± 0.2	ND
C20:3n-6	0.1 ± 0.2	0.1 ± 0.2	0.4 ± 0.3	ND
C20:4n-6	3.0 ± 1.0	3.4 ± 1.5	3.9 ± 0.2	3.6 ± 0.1
C22:6n-3	3.4 ± 0.9	3.6 ± 1.0	3.1 ± 0.7	3.5 ± 0.3
Total	59.3 ± 35.9	50.3 ± 28.1	102.7 ± 22	51.8 ± 14.9

Values are means ± SD; $n = 6$ mice per group. ND, not detected (μg/mg). a1–a2 and b, vs. wild-type mice (HFD); $^{a1-a2}P < 0.05$; $^{b}P < 0.02$ (Student's *t*-test).

Furthermore, a 30.2% reduction of phosphorylated Smad 3, representing lower myostatin signaling, was detected in skeletal muscles but not in other tissues (Fig. 3*B*). Therefore, it is likely that myostatin signaling in muscle, rather than the direct effects of myostatin on adipose tissue, is responsible for the decrease in fat mass in FS I-I Tg mice. We also studied the effects of myostatin and FS I-I in Hep G2 cells and 3T3-L1 cell lines. In both cases, the triglyceride level was not affected either by myostatin or by follistatin-derived peptide stimulation (Fig. S4), supporting the secondary and indirect effects of FS I-I on adipocytes and hepatocytes. The increased skeletal muscle mass may have greater capacity for glucose uptake, reducing substrate supply for hepatic lipogenesis.

The normal age-dependent adipose tissue accumulation was decreased in NFD-fed FS I-I Tg mice (Fig. 1*A*). Intriguingly, the adipocytes were smaller as a result of myostatin inhibition by FS I-I (Fig. 1, *B–D*), reflecting reduced lipid accumulation. Obesity occurs when the adipose tissue is overloaded with high-energy nutrients and energy expenditure is reduced. Therefore, we studied the effect of diet-induced obesity in FS I-I Tg and wild-type mice. The body weight of HFD-fed FS I-I Tg mice was comparable with that of HFD-fed wild-type mice (Fig. 4*A*), which was attributed to the increase in muscle weight and decrease in adipose tissue and liver weights in FS I-I Tg mice (Fig. 4, *B* and *C*). Interestingly, there is a report that mice with an insertion allele at the *Inhba* locus, $Inhba^{BK}$, are smaller and leaner than wild-type littermate (20). In $Inhba^{BK}$ mice, the sequences of the mature activin-βA domain were replaced with the corresponding sequences from activin-βB. $Inhba^{BK}$ mice have less adipose tissue than wild-type littermates. The growth of $Inhba^{BK}$ is improved by providing an HFD to a level comparable with that of wild-type mice on an NFD (20). The phenotype of FS I-I mice with lower myostatin signaling is different from that of $Inhba^{BK}$ mice. Therefore, although activin A and myostatin are functionally similar to maintain energy balance and regulate skeletal muscle mass, they may have different functions in vivo. As would be expected, the HFD increased the levels of cholesterol, fasting glucose, insulin, and leptin (Fig. 4*D* and Table 1) compared with the NFD in wild-type mice (Table 1). However, the triglyceride, NEFA, cholesterol, insulin, and leptin levels were lower in HFD-fed FS I-I Tg mice than in HFD-fed wild-type mice (Table 1 and Fig. 4*D*). Furthermore, we observed an increase in serum adiponectin in FS I-I Tg mice (Table 1). These results are similar to those of myostatin-null mice and myostatin propeptide Tg mice (13, 42). Interestingly, the HFD-fed FS I-I Tg mice exhibited better glucose tolerance than HFD-fed wild type mice (Fig. 4*E*). By contrast, in mice fed the NFD, glucose tolerance was similar in FS I-I Tg and wild-type mice. This differs from the situation in myostatin knockout mice, because myostatin knockout mice showed improved glucose tolerance, even when they were fed the NFD (24). With respect to whole body metabolism, we performed indirect calorimetric analyses. Although food intake was not significantly different between wild-type and FS I-I mice, the metabolic rate calculated from $\dot{V}o_2$ was increased in FS I-I Tg compared with control. When normalized with body weight, no statistically significant difference was observed (Supplementary Table S1). Collectively, these results indicate that FS I-I Tg mice were resistant to HFD-induced obesity and showed improved glucose tolerance during excess energy intake.

Intriguingly, FS I-I Tg mice were resistant to hepatic steatosis during high-fat feeding, which was confirmed by histology, liver weight, and liver fatty acid accumulation (Fig. 5, *A–C* and Table 2). The hepatic histology of HFD-fed FS I-I Tg mice did not show any difference to NFD-fed wild-type mice. The hepatic expression level of SCD1 mRNA was lower in FS I-I Tg mice than in wild-type mice. SCD1 is a rate-limiting lipogenic enzyme required for the synthesis of monounsaturated fatty acids and plays a key role in the hepatic synthesis of triglycerides. As a result of decreased SCD1 expression, the hepatic content of oleic acid (C18:1) and palmitoleic acid (C16:1), monounsaturated fatty acids produced by SCD1, was decreased (Fig. 6*B* and Table 2). A decrease in SCD1 expression was reported to be responsible for the prevention of diet-induced obesity, insulin resistance, and diabetes (9, 28). Furthermore, SCD1-null mice were resistant to diet-induced obesity and hepatic steatosis (9). The resistance of FS I-I Tg mice to HFD-induced obesity and hepatic steatosis may, in part, involve the reduced mRNA expression of SCD1. Changes of RNA and protein end points represent lower adiposity and lower hepatic fat levels. The lower adiposity is likely secondary to increased muscle mass and lower myostatin signaling in skeletal muscle.

The increase in skeletal muscle mass and reduction in fat mass would likely take at least several months to occur. Meanwhile, injection of myostatin neutralizing antibody does not decrease the adipose tissue mass (35, 39). However, even if the fat mass is not decreased, it seems likely that the inhibition of myostatin improves glucose tolerance and insulin sensitivity and prevents hepatic steatosis due to lower insulin levels, increased adiponectin levels, and changes in substrate utilization in skeletal muscle, adipose tissue, and liver. In summary, the inhibition of myostatin by various strategies, including follistatin-derived peptide, may offer a novel therapy against obesity, diabetes, and hepatic steatosis.

ACKNOWLEDGMENTS

We thank Drs. K. Hitachi, A. Uezumi, and H. Ageta for discussion and advice. We also thank S. Sato and A. Yamaguchi for technical assistance.